

In search of radio emission from exoplanets: GMRT observations of the binary system HD 41004

Mayank Narang^{1,*}, P. Manoj¹, C. H. Ishwara Chandra², Joseph Lazio³,
Thomas Henning⁴, Motohide Tamura^{5,6,7}, Blesson Mathew⁸,
Nitish Ujwal⁹, Pritha Mandal⁸

¹Tata Institute of Fundamental Research Homi Bhabha Road, Colaba, Mumbai 400005, India

²National Centre for Radio Astrophysics, TIFR, Post Bag 3, Ganeshkhind, Pune 411007, India

³Jet Propulsion Laboratory, California Institute of Technology, Pasadena CA 91106, United States

⁴Max-Planck-Institut für Astronomie, Königstuhl 17, D-69117 Heidelberg, Germany

⁵The University of Tokyo, 7-3-1, Hongo, Bunkyo-ku, Tokyo, 113-0033, Japan

⁶Astrobiology Center, 2-21-1, Osawa, Mitaka, Tokyo 181-8588, Japan

⁷National Astronomical Observatory of Japan, 2-21-1 Osawa, Mitaka, Tokyo 181-8588, Japan

⁸Department of Physics and Electronics, CHRIST (Deemed to be University), Bangalore, Karnataka - 560034

⁹Indian Institute of Technology Bombay, Powai, Mumbai, 400076, India

16 November 2020

ABSTRACT

This paper reports Giant Metrewave Radio Telescope (GMRT) observations of the binary system HD 41004 that are among the deepest images ever obtained at 150 MHz and 400 MHz in the search for radio emission from exoplanets. The HD 41004 binary system consists of a K1 V primary star and an M2 V secondary; both stars are host to a massive planet or brown dwarf. Analogous to planets in our solar system that emit at radio wavelengths due to their strong magnetic fields, one or both of the planet or brown dwarf in the HD 41004 binary system are also thought to be sources of radio emission. Various models predict HD 41004Bb to have one of the largest expected flux densities at 150 MHz. The observations at 150 MHz cover almost the entire orbital period of HD 41004Bb, and about 20% of the orbit is covered at 400 MHz. We do not detect radio emission, setting 3σ limits of 1.8 mJy at 150 MHz and 0.12 mJy at 400 MHz. We also discuss some of the possible reasons why no radio emission was detected from the HD 41004 binary system.

Key words: Stars: planetary systems – Stars: individual: HD 41004 – Techniques: interferometric radio

1 INTRODUCTION

In the last two decades, the exoplanet population has increased substantially. There have been several studies aimed at measuring and characterizing the properties of exoplanets and their dependence on host star properties (e.g., Gonzalez 1997; Cumming et al. 2008; Perryman 2011; Batalha et al. 2013; Gaidos et al. 2013; Marcy et al. 2014; Dressing & Charbonneau 2015; Mulders et al. 2015; Winn & Fabrycky 2015; Narang et al. 2018; Mulders 2018; Shkolnik & Llama 2018; Winn 2018; Viswanath et al. 2020). Still, one of the remaining and a very challenging task in exoplanet research is determining the interior structures and compositions of exoplanets, for which the detection of magnetic fields would provide important constraints. Radio emission

is probably the only way to detect magnetic fields of exoplanets unambiguously (Grießmeier 2015). It places not only strong constraints on the exoplanet magnetic fields but also provides important clues to their internal structure (e.g., Sánchez-Lavega 2004; Reiners & Christensen 2010; Lazio et al. 2019). All planets in our solar system that possess a strong magnetic field also emit at radio wavelengths (e.g., Burke & Franklin 1955; Bigg 1964; Zarka 1998, 2000). Exoplanets with strong magnetic fields are also thought to emit strongly at radio wavelengths (e.g., Zarka et al. 1997; Farrell et al. 1999; Zarka et al. 2001; Lazio 2018; Zarka 2018; Grießmeier 2018).

Planets in our solar system emit radio emission via the electron cyclotron maser instability (ECMI) mechanism (e.g., Wu & Lee 1979; Zarka et al. 1997; Zarka 1998, 2000; Treumann 2006; Louis et al. 2019). According to this mechanism, energetic electrons gyrate and accelerate along the

* E-mail: mayank.narang@tifr.res.in

magnetic field lines of planets (to which they are confined) and produce radio emission (Melrose & Dulk 1982; Dulk 1985). This emission is highly circularly polarized. The radio emission from exoplanets is also thought to follow a similar mechanism.

ECMI requires three components: (i) a magnetic field; (ii) a source of energetic (keV) electrons; and (iii) anisotropy in the electron distribution function. According to the Radiometric Bode’s law, the radio power from the planet P_{rad} , is directly proportional to the input power P_{in} , supplied to the electrons (e.g., Desch & Kaiser 1984; Zarka et al. 1997; Farrell et al. 1999). The primary mechanisms that can input power to the electrons and hence supply the energetic electrons for ECMI are *Stellar Wind Kinetic Energy*, *Stellar Wind Magnetic Energy*, *Coronal Mass Ejection* (CME), and *Unipolar interaction* (Zarka et al. 2001; Grießmeier et al. 2007b; Lazio 2018; Zarka et al. 2018).

There have been several studies aimed at detecting the radio emission from exoplanets (see Grießmeier 2017 and Lazio 2018 for up to date reviews, along with Bastian et al. 2018, O’Gorman et al. 2018, Lynch et al. 2018, and Route 2019). However, none of them have been successful in directly detecting radio emission from exoplanets. Recently Vedantham et al. (2020) have reported the detection of radio emission from an M dwarf star, GJ 1151. The detected radio emission from GJ 1151 is consistent with ECMI expected from a planet. Vedantham et al. (2020) model the emission properties to show that the emission is consistent with the theoretical expectations for host star interaction with an Earth-size planet with a one-to-five-day orbital period. However, follow-up radial velocity studies have not been able to detect the planet but have placed upper limits of a few times the mass of the Earth (Pope et al. 2020), which is consistent with their models for radio emission.

This paper presents our analysis of the radio observations of the binary system HD 41004 using the Giant Metrewave Radio Telescope (GMRT). HD 41004Bb is thought to be the best candidate to observe radio emission from an exoplanet with an estimated flux density of 910 mJy and with a maximum emission frequency of 140 MHz (Grießmeier 2017). HD 41004Bb also has a period of only 32 hrs, making observations of its entire orbit possible. The large expected flux density at a low frequency of 150 MHz (close to the expected maximum cyclotron frequency), along with the short orbital period, makes HD 41004Bb an excellent candidate to observe with GMRT. We used legacy GMRT data (retrieved using the GMRT online archive)¹ along with observations with the upgraded GMRT (uGMRT) to produce the deepest images of the HD 41004 field at 150 MHz and 400 MHz. In Sect. 2, we describe the HD 41004 system. The observations and data analysis are described in Sect. 3. We present our results in Section 4 and discuss them in Section 5.

2 TARGET

HD 41004 is a $\sim 1.6 \pm 0.8$ Gyrs old (Saffe et al. 2005) binary system located 41.5 pc (Bailer-Jones et al. 2018; Gaia

DR2 Collaboration et al. 2018) away from Earth. The system is host to a K1 V primary (HD 41004A) star, and an M2 V secondary star (HD 41004B) that are separated by 0.5” (21 AU). HD 41004A hosts a Jupiter-like planet with a projected mass of $2.5 M_{\text{J}}$ at 1.7 AU from the host star (Zucker et al. 2004). HD 41004B, on the other hand, is host to a massive companion with a projected mass of $18.4 M_{\text{J}}$, HD 41004Bb, at an orbital distance of 0.018 AU (orbital period = 32 hrs) (Zucker et al. 2004). Since these planets are detected only via the radial velocity method, the masses given above are lower limits $M \sin i$, and the true mass of the planets are likely to be higher. This might affect some of the estimates of maximum cyclotron frequency and expected flux density. Furthermore, the projected mass of HD 41004Bb is $18.4 M_{\text{J}}$, which is greater than $13 M_{\text{J}}$, the planet/brown dwarf boundary, which makes HD 41004Bb a low mass brown dwarf. However, the same radio emission mechanism of ECMI is thought to operate for brown dwarfs and exoplanets (e.g., Antonova et al. 2007; Hallinan et al. 2007; Hallinan et al. 2008).

2.1 Emission frequency

The maximum cyclotron frequency for radio emission from the planet is a function of the surface magnetic field of the planet at the pole and is given as:

$$\nu_{\text{c}} = 2.8 \text{ MHz } [B_{\text{P}}/\text{G}] \quad (1)$$

where B_{P} is the polar magnetic field strength of the planet in Gauss. We approximate the polar surface magnetic field for an exoplanet as a function of planet mass M_{P} , planet radius R_{P} , and its rotation rate ω_{P} (For further details see the Appendix A):

$$B_{\text{P}} = 8.4 \text{ G } \left(\frac{\omega_{\text{P}}}{\omega_{\text{J}}} \right) \left(\frac{M_{\text{P}}}{M_{\text{J}}} \right) \left(\frac{R_{\text{J}}}{R_{\text{P}}} \right) \quad (2)$$

where the planet mass, planet radius, and rotation rates are normalized with respect to that of Jupiter. This gives

$$\nu_{\text{c}} = 2.8 \text{ MHz } [B_{\text{P}}/\text{G}] = 23.5 \text{ MHz } \left(\frac{\omega_{\text{P}}}{\omega_{\text{J}}} \right) \left(\frac{M_{\text{P}}}{M_{\text{J}}} \right) \left(\frac{R_{\text{J}}}{R_{\text{P}}} \right) \quad (3)$$

Based on its proximity to the host star, HD 41004Bb is likely to be tidally locked such that its rotation period and the orbital period are the same (see Gladman et al. 1996, for the time scale of tidal locking). Using the values for HD 41004Bb ($M_{\text{P}} = 18.4 M_{\text{J}}$, period = 32 hrs and a radius $R_{\text{P}} = 1.08 R_{\text{J}}$ using the mass-radius relationship from Chen & Kipping (2017)) in equation (3), we find the maximum cyclotron frequency to be 125 MHz. With a bandwidth of emission $\Delta\nu \sim \nu_{\text{c}}/2$ (Lazio & Farrell 2007; Grießmeier et al. 2007b, 2011) the emission should be observable in band 2 (150 MHz) of GMRT.

Equation (2) used to estimate the magnetic field strength is based on the scaling relations derived from the planets in our solar system. These scaling relations might not be applicable in the case of close-in planets. Yadav & Thorngren (2017) have argued that the magnetic fields of close-in hot-Jupiters could be ~ 10 times that predicted using the scaling laws. Higher values of magnetic fields would

¹ naps.ncra.tifr.res.in/goa/data/search

result in the maximum cyclotron frequency of the emission going up. More conservatively, if B_P is 2 to 4 times that predicted by equation (2), that would correspond to maximum emission frequency ranging from 250-500 MHz. The emission then would fall within band 3 (250-500 MHz) of uGMRT. Moreover, a peak cyclotron frequency of 400 MHz also corresponds to the case of the planet not being tidally locked and having a rotation rate similar to that of Jupiter (10 hrs).

HD 41004Ab, on the other hand, is at 1.7 AU from the host star and has a $M \sin i$ of $2.5 M_J$. Given that the projected mass of HD 41004Ab is within a few factors of Jupiter, we might expect that its magnetic field is comparable to that of Jupiter. Consequently, it would emit at frequencies below 100 MHz (see equation 3) and would not emit at frequencies detectable by the GMRT.

2.2 Modeling the emission

The predicted radio flux density, S_{rad} , of an exoplanet is given as (Farrell et al. 1999; Lazio et al. 2004; Grießmeier et al. 2007b):

$$S_{\text{rad}} = \frac{P_{\text{rad}}}{\Delta\nu \Omega d^2} \quad (4)$$

where P_{rad} , is the radio power emitted by the exoplanet, $\Delta\nu$ is the bandwidth of emission, Ω , the angle of the emission cone, and d is the distance of the exoplanet from Earth. Based on the studies of the radio emission from solar system planets, it has been shown that the radio power P_{rad} , from the planets, is proportional to the incident/input power from the solar wind, i.e., $P_{\text{rad}} = \eta P_{\text{in}}$, where P_{in} is the input power and η is a proportionality constant which takes care of power that is deposited in the planets and the conversion efficiency of the deposited power to radio power. The proportionality constant η is derived by equating the input power for Jupiter (for the various input power models) with the observed average radio power from Jupiter during periods of high activity (Grießmeier et al. 2007b; Lynch et al. 2018).

There are several mechanisms by which the input power from the stellar wind can be supplied to the planet, as discussed in Section 1. Below we discuss the two prominent mechanisms for the input power (e.g., Grießmeier et al. 2007b; Lazio 2018; Lynch et al. 2018; Zarka et al. 2018):

(i) *Stellar Wind Kinetic Energy*: The kinetic energy of the protons in the stellar wind impinging on the planet's magnetosphere provides the input power. The input power is proportional to the number density of the stellar wind, n , at the location of the planet and the cube of the effective velocity of the stellar wind at the location of the planet, $v_{\text{eff}} = \sqrt{v_*^2 + v_k^2}$, where v_* is the stellar wind velocity at the location of the planet calculated using the Parker's isothermal solution (Parker 1958; Grießmeier et al. 2007b) and v_k is the Keplerian velocity of the planet.

$$P_{\text{in}} \propto n v_{\text{eff}}^3 \quad (5)$$

(ii) *Stellar Wind Magnetic Energy*: The magnetic flux or the electromagnetic Poynting flux from the interplanetary

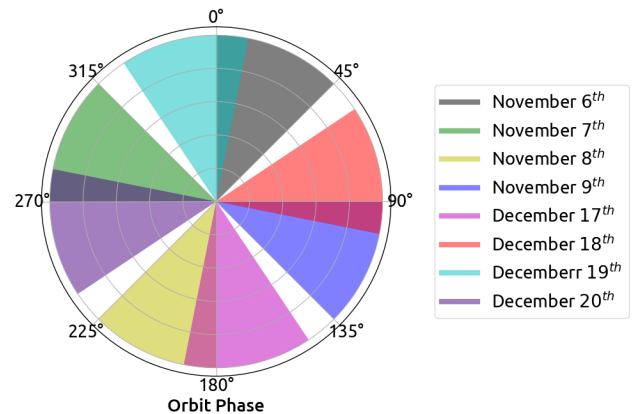


Figure 1. The orbit phase coverage for HD 41004Bb during the GMRT observations at 150 MHz. We have assumed a phase of 0 at the beginning of the observation and then calculated the planet's phase at subsequent nights. The different colors circle correspond to different nights.

magnetic field incident on the planet's magnetosphere provides the power input. The input power, in this case, is proportional to the square of the strength of the interplanetary magnetic field perpendicular to the stellar wind flow, B_{\perp} at the location of the planet (following Zarka 2007; Grießmeier et al. 2007b, with the assumption that the stellar magnetic field strength is similar to that of the Sun) and effective velocity of the stellar wind, v_{eff}

$$P_{\text{in}} \propto B_{\perp}^2 v_{\text{eff}} \quad (6)$$

Recently, by studying the radio emission from the interaction between Jupiter and Ganymede and Jupiter and Io Zarka et al. (2018) (also see Zarka et al. (2017) and Grießmeier (2018)) have shown that the emitted radio power is proportional to the Poynting flux from Jupiter's magnetosphere intercepted by Io or Ganymede. When combined with the scaling of radio power as a function of the incident magnetic power for planets in our solar system, this result indicates that the *Stellar Wind Magnetic Energy* is the dominant mechanism that supplies the input energy for radio emission. However, since for the planets in our solar system, both the *Stellar Wind Kinetic Energy* and the *Stellar Wind Magnetic Energy* model give the same qualitative results (Zarka 2007; Zarka et al. 2018), we have opted to investigate both models.

We model the flux density for HD 41004Bb at 125 MHz and 400 MHz using the two above mechanisms. Taking the distance to the system from Bailer-Jones et al. (2018) of 41.5 pc, $\Delta\nu = \nu_c/2$ and $\Omega = 1.6 \text{ sr}$ (Zarka et al. 2004) and making use of equations (4), (5) and (6) we calculate the expected flux density from HD 41004Bb. For the maximum cyclotron frequency of 125 MHz, the expected flux density from the *Stellar Wind Kinetic Energy* model is 3 mJy. At the same time, the expected flux density based on the *Stellar Wind Magnetic Energy* model is 64.0 mJy. For the maximum cyclotron frequency of 400 MHz the predicted flux density from the *Stellar Wind Kinetic Energy* is 2.0 mJy and from the *Stellar Wind Magnetic Energy* model the predicted flux density is 44 mJy.

The flux density estimates from our models are significantly lower than that from [Grießmeier \(2017\)](#) ($S_{rad} = 910$ mJy with maximum emission frequency $\nu_c=140$ MHz), who, following [Grießmeier et al. \(2007a\)](#) and [Grießmeier et al. \(2011\)](#), estimated the flux density from HD41004Bb using the Stellar Wind Magnetic Energy model. [Grießmeier \(2017\)](#) have has use of several empirical relations (from, e.g., [Newkirk 1980](#); [Grießmeier et al. 2004, 2007b](#)) that relate the age of the host star to the stellar wind velocity, the number density of protons in the stellar wind, stellar rotation rate, and magnetic field of the star for modeling the flux densities. Since individual age measurements of main sequence stars are difficult, and the HD 41004 system’s age is very uncertain (1.6 ± 0.8 Gyrs), we do not use these relations in our modeling. However, if we also make similar assumptions as made by [Grießmeier \(2017\)](#), we get a similar value for the predicted flux density at with a maximum emission frequency of 125 MHz.

3 OBSERVATION AND DATA ANALYSIS

The HD 41004 field was observed on multiple nights in November and December 2009, with the legacy GMRT. The field was observed at 150 MHz, with a bandwidth of 6 MHz. In order to ensure the full rotational phase coverage of HD 41004Bb, the field was observed in two observing blocks consisting of four successive nights in each block (2009 November 6th, 7th, 8th, 9th and 2009 December 17th, 18th, 19th, 20th), with ~ 4 hours observing per night (see Figure 1).

For each of the eight observations, the phase center was set at the position of HD 41004. The quasars 3C147 and 3C48 were used as the flux and band-pass calibrator. The band-pass and flux calibrators were observed twice, at the beginning and the end of the observations. We used 0616-349 as the phase calibrator. It was observed at frequent intervals during the observations in a loop of 27 min on the source, HD 41004, and 5 min on the phase calibrator, 0616-349.

To reduce the data, the Source Peeling and Atmospheric Modeling (SPAM) pipeline ([Intema et al. 2009](#); [Intema 2014a,b](#)) was used. SPAM is an automated pipeline for reducing legacy GMRT observations at 150, 235, 325, and 610 MHz. SPAM includes direction-dependent calibration, modeling, and imaging for correcting ionospheric dispersive delay. The pipeline first converts the raw data (LTA or Long Term Accumulation format) to precalibrated visibility sets and then converts these precalibrated visibility sets into Stokes I continuum images.

We further carried out observations with the upgraded GMRT (uGMRT) in band 3 (250-500 MHz). The uGMRT observations of the HD 41004 field were made on 2018 October 30 and 31. The center frequency of the receiver was set at 400 MHz, with a bandwidth of 200 MHz. For each observation, the phase center was set at the position of HD 41004. 3C147 was observed as the primary flux density and band-pass calibrator twice during the observation, once at the beginning and once at the end. The phase calibrator used was 0616-349 and was observed for 5 minutes after 30 minutes on the target in a loop.

The data were reduced using CASA with the uGMRT pipeline ([Ishwara-Chandra et al. 2020](#)). Initial flagging was

carried out using the CASA task *flagdata*. After flagging, the delay, band-pass, and gain calibration were performed. The initial calibration was then removed, and the data were flagged again. After this, we re-calibrated the data. Then the imaging of the science target was carried out using the task *tclean* in CASA. Four rounds of phase-only self-calibration with reducing solution intervals of 8, 4, 2, and 1 minute(s) were carried out. After convergence of phase-only self-calibration, five rounds of amplitude and phase self-cal with solution intervals of 8, 4, 2, 1, and 1 minute(s) were performed. From the first to last round of self-calibration cycle in both phase-only and amplitude and phase self-calibration, the number of clean iterations were doubled along with the lowering of clean threshold resulting in deeper images in subsequent cycles. In between each self-calibration iteration, flagging based on residuals was performed, which improved image quality in each cycle (see [Ishwara-Chandra et al. \(2020\)](#) for more details). Afterward, a primary beam correction to the image was also applied using the CASA task *wbpbgmt*² to produce the final image.

4 RESULTS

No radio emission was detected from either HD 41004Ab or HD 41004Bb at 150 MHz or 400 MHz. The HD 41004 field was observed at 150 MHz with the legacy GMRT for eight nights with ~ 4 hrs of observations per night, totaling to 32 hrs of observation time. No emission was detected for each of the ~ 4 hr observations. The rms values achieved for each of the eight nights are listed in Table 1, and the images are shown in Figure 2. To make a deeper image, we combined the eight observations. We were able to achieve an rms of 0.8 mJy after 32 hrs of observations. However, if we exclude the observations from 2009 November 6th, 2009 November 7th, and 2009 December 20th, which have rms higher than the median rms for the eight nights, we produce an image with an rms of 0.6 mJy. This is shown in Figure 3. This rms is similar to the lowest rms achieved with GMRT for an exoplanet field at 150 MHz ([Hallinan et al. 2013](#)) (also see Figure 5).

We also observed the HD 41004 system in band 3 (250-500 MHz) with uGMRT at 400 MHz with a bandwidth of 200 MHz. An advantage of observing in band 3 (250-500 MHz) with uGMRT is that it offers better sensitivity than that can be obtained in band 2 (150 MHz) of GMRT ([Gupta et al. 2017](#)). No radio emission was detected from the HD 41004 systems on either of the nights. From our uGMRT observations, we obtained an rms of 40 μ Jy on the night of October 30th and an rms of 70 μ Jy on October 31st at 400 MHz after 3 hrs of observations on each night. The final images are shown in Figure 4(a) and Figure 4(b).

Our observations reached sensitivities that could have easily resulted in detection, yet no emission was detected toward HD 41004Bb. At the maximum emission frequency of 150 MHz, the *Stellar Wind Magnetic Energy* model predicts a flux density of 64 mJy, while the achieved 3σ sensitivity is 1.8 mJy. Similarly, at the maximum emission frequency

² <https://github.com/ruta-k/uGMRTprimarybeam>

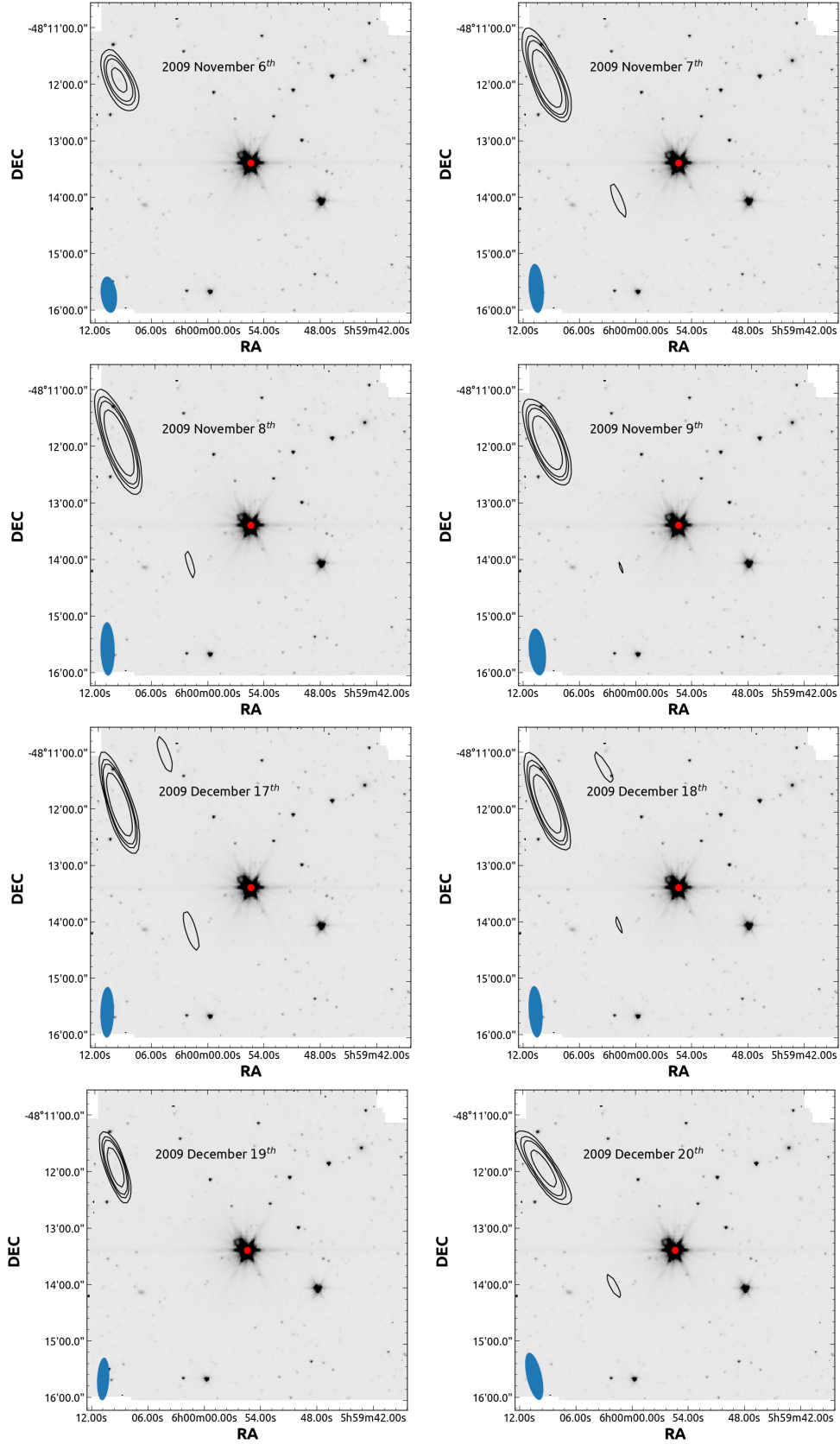


Figure 2. The legacy GMRT image of the HD 41004 field at 150 MHz for each of the individual nights of observation overlaid on the Spitzer IRAC 1 ($3.6 \mu\text{m}$) image of the HD 41004 field in greyscale. The red solid circle marks the position of the HD 41004 system. The contours plotted are $5, 10, 15,$ and $30 \times \sigma$. The beam is shown as a blue ellipse at the bottom left corner.

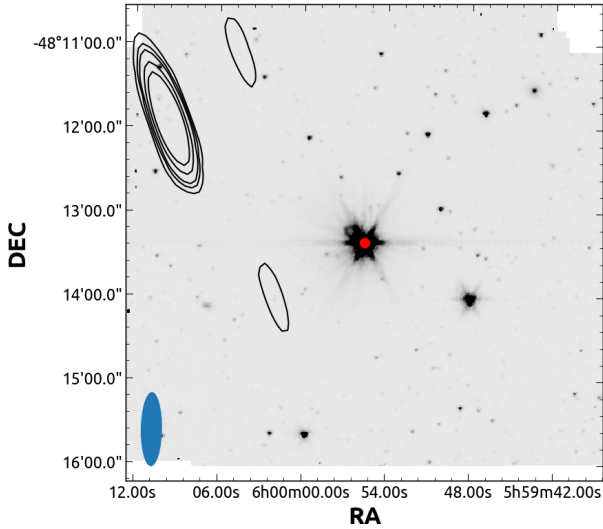


Figure 3. The legacy GMRT image of the HD 41004 field at 150 MHz after combining the observations from November 8th, November 9th, December 17th, December 18th, and December 19th overlaid on the Spitzer IRAC 1 ($3.6 \mu\text{m}$) image of the HD 41004 field in greyscale. The solid red circle marks the position of the HD 41004 system. The contours plotted are 5, 10, 15, 30, $50 \times \sigma$ with $\sigma = 0.6 \text{ mJy}$. The beam is shown as a blue ellipse at the bottom left corner. At this scale, we cannot resolve HD 41004A and HD 41004B.

of 400 MHz, the predicted flux density (based on the *Stellar Wind Magnetic Energy* model) is 44 mJy, while the 3σ sensitivity achieved was 0.12 mJy (also see Table 2).

Using the observed flux density upper limits, we can place limits on the radio power emitted by the HD 41004Bb system. These calculations are based on the assumption that there is a steady-state quiescent component to the emission and that the Earth was in the emission cone of the planet during the observations. Using Equation 4 and assuming the solid angle of the beamed emission, $\Omega = 1.6 \text{ sr}$ (Zarka et al. 2004) and $\Delta\nu = \text{observed frequency}/2$, the upper limit to radio power at 150 MHz is $3.5 \times 10^{15} \text{ W}$. At 400 MHz, the upper limit to radio power is $6 \times 10^{14} \text{ W}$. These upper limits are about 3 to 4 orders higher than the average power during periods of high activity from Jupiter $P_{\text{rad}} = 2.1 \times 10^{11} \text{ W}$ (Zarka et al. 2004).

5 DISCUSSION

We have made some of the deepest observations at 150 MHz and 400 MHz of an exoplanet field. In Figure 5, we compare rms sensitivities of observations that have been carried out to detect radio emission from exoplanets. Also shown is the detection of radio emission from the system GJ 1151 by Vedantham et al. (2020) as a magenta downwards triangle. The flux density from GJ 1151 (0.89 mJy) is comparable to the rms flux density (0.6 mJy) we achieved at band-2 (150 MHz).

In the following subsection, we discuss possible reasons why no radio emission was detected from HD 41004Bb and

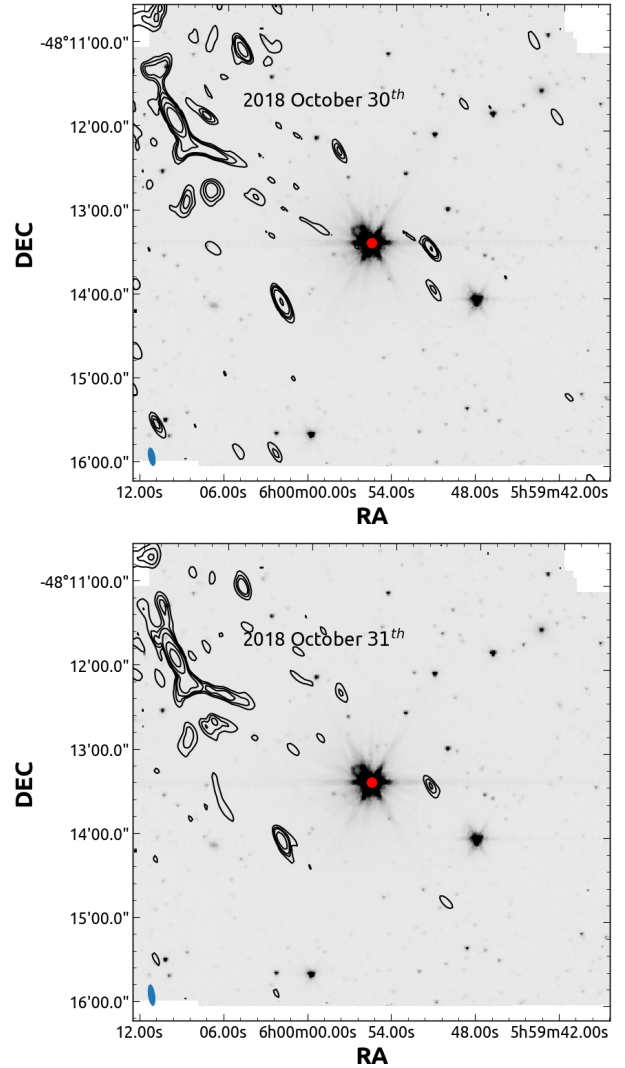


Figure 4. The radio image of the HD 41004 field at 400 MHz for two different nights 2018 October 30 (a) and 2018 October 31 (b). These images are overlaid on the Spitzer IRAC 1 image of the HD 41004 field in grey scale. The red solid circle marks the position of HD 41004 system. The contours plotted are 5, 10, 15, 30, 100 and $300 \times \sigma$ where $\sigma = 40 \mu\text{Jy}$ for the night of October 30 and $\sigma = 70 \mu\text{Jy}$ for the night of October 31. The beam is shown as a blue ellipse at the bottom left corner.

how our deep observations allow us to place critical constraints on various radio emission mechanisms.

5.1 Overestimation of flux and saturation of emission

One of the reasons why we did not detect any radio emission could be that the radio emission is too weak at these frequencies, and the models of the emission mechanisms might need further revisions. To calculate the expected flux density, several assumptions, and scaling relationships had to be used (to calculate, e.g., the stellar wind proton density, the stellar wind speed, stellar magnetic field). These assumptions and scaling relationships are based on the Sun. If these relation-

Band	Date	Central Frequency (MHz)	Bandwidth (MHz)	Observation time (hrs)	Image RMS (mJy/beam)
2	2009 November 6 th	150	6	4	2.1
2	2009 November 7 th	150	6	4	1.2
2	2009 November 8 th	150	6	4	0.9
2	2009 November 9 th	150	6	4	1.0
2	2009 December 17 th	150	6	4	1.1
2	2009 December 18 th	150	6	4	1.1
2	2009 December 19 th	150	6	4	1.0
2	2009 December 20 th	150	6	4	1.7
2	Combining all	150	6	32	0.8
2	Combining observations from 2009 November 8 th , November 9 th , 2009 December 17 th , December 18 th , and December 19 th	150	6	20	0.6
3	2018 October 30 th	400	200	3	0.04
3	2018 October 31 th	400	200	3	0.07

Table 1. Summary of the observations and the combined images.

ships and assumptions do not hold for an M type star, the modeled flux densities might be incorrect.

Further, [Jardine & Collier Cameron \(2008\)](#) suggested that close-in planets might lie inside the magnetosphere of the star. Due to this, the magnetospheres of these close-in planets are determined by the magnetic pressure of the stellar magnetosphere and not by the ram pressure of the stellar wind. As the planetary orbital distance decreases, the electron density ρ_e rises, so the number of available electrons increases. However, this is exactly balanced by the shrinking of the planet’s magnetosphere, which reduces the cross-section of the planet available for radio emission ([Jardine & Collier Cameron 2008](#)). This may result in the saturation of the output power, even while the input power increases.

In hot-Jupiter, the magnetospheric convection may saturate, and, hence, they may not dissipate the total incident’s magnetic energy from the stellar wind ([Nichols & Milan 2016](#)). Due to this, the emission from these hot-Jupiters may not follow the Radiometric Bode’s Law, and the expected flux densities would be overestimated.

If this is the case, the observed flux density upper limits that we derive in Section 4 can be used to constrain by how much the constant of proportionality η (that relates input power to radio power) for HD 41004Bb differs from that of Jupiter. The proportionality constant, η , used in calculating the expected flux densities, was obtained by comparing the estimated input power to Jupiter (for the two models) with

the observed radio power from Jupiter. However, η could be different for HD 41004Bb. An upper limit to the ratio of η_{HD} (constant of proportionality for HD 41004Bb) and η_J (constant of proportionality for Jupiter) can be calculated as a multiplicative factor κ_{\max} , by dividing the observed 3σ flux density upper limits, $S_{3\sigma}$ with the modeled flux density, S_{rad} such that:

$$\frac{\eta_{HD}}{\eta_J} = \kappa_{\max} = \frac{S_{3\sigma}}{S_{\text{rad}}} \quad (7)$$

In Table 2 we summarise the values of the predicted flux density for the two models (*Stellar Wind Kinetic Energy* and *Stellar Wind Magnetic Energy*) for the two peak emission frequencies that we have considered along with the 3σ rms sensitivity achieved and the values of κ_{\max} . The value of κ_{\max} is between 0.003 to 0.6 for the different models/hypotheses we have considered in this study.

5.2 Incorrect maximum cyclotron frequency estimates

For HD 41004Bb, the maximum cyclotron frequency, assuming tidal locking, is 125 MHz. Recently, however, [Yadav & Thorngren \(2017\)](#) have argued that due to the inflation of hot-Jupiters, their magnetic fields can be much stronger than that predicted using scaling laws that do not take the heating of these planets into account. Stronger magnetic

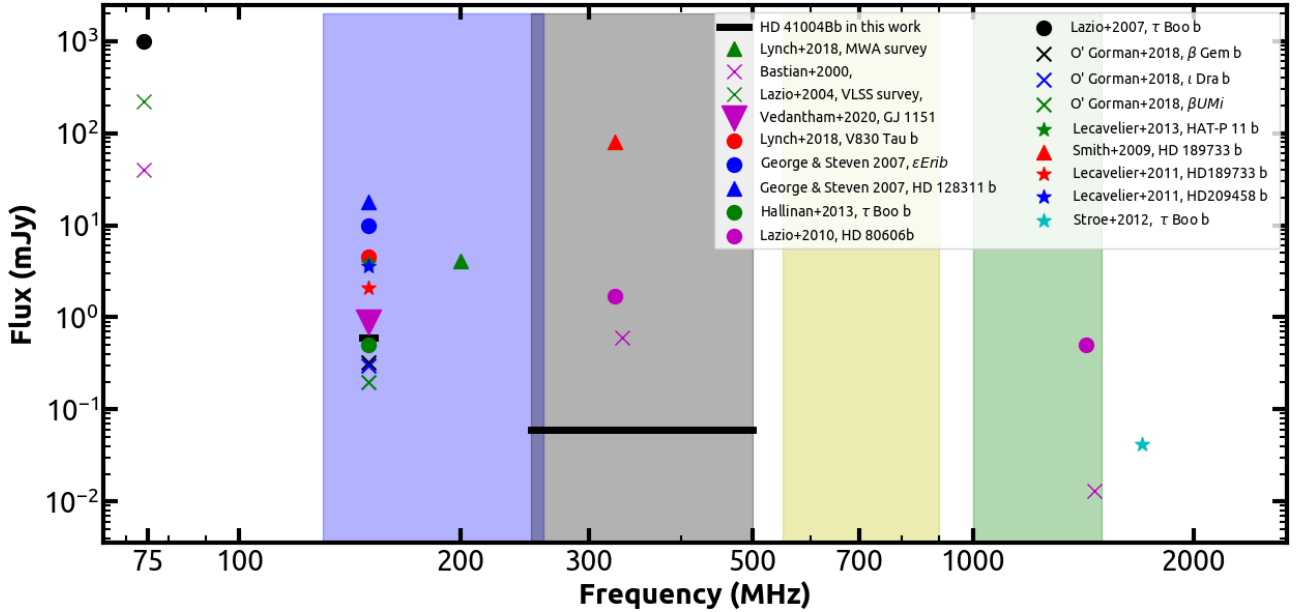


Figure 5. The rms flux densities for some of the previous attempts at detecting radio emission from exoplanets as a function of the frequency of observations (Lazio et al. 2004; Lynch et al. 2018; Bastian et al. 2000; Lazio & Farrell 2007; George & Stevens 2007; Hallinan et al. 2013; O’Gorman et al. 2018; Lecavelier des Etangs et al. 2013; Lecavelier Des Etangs et al. 2011; Lazio et al. 2010; Smith et al. 2009; Stroe et al. 2012) along with the rms sensitivity we reached in this work (black solid line) for the 150MHz and 400 MHz uGMRT observations. Also shown is the detection of radio emission from the system GJ 1151 by Vedantham et al. (2020). The uGMRT bands are shown in different colors (blue band 2 (120-250 MHz), grey band 3 (250-500 MHz), yellow band 4 (550-900 MHz), and green band 5 (1000-1450 MHz)).

fields imply higher frequency than predicted using empirical relations previously used in various studies. Furthermore, if the planet is weakly magnetized, the emission would be at a much lower frequency.

5.3 Variable/Episodic emission

The low-frequency radio emission from the solar system planets is highly variable over time. For example, Jupiter’s decameter emission varies on timescales of several minutes and can produce emissions that are ten times higher than the median level (Zucker et al. 2004; O’Gorman et al. 2018). The radio emission from exoplanets could also be episodic. Episodic radio bursts have been seen from isolated brown dwarfs (e.g. Berger et al. 2001; Hallinan et al. 2008; Wolsczan & Route 2014; Kao et al. 2016; Williams et al. 2017). The emission from GJ 1151 is also variable (Vedantham et al. 2020), and hence long term monitoring of exoplanet hosts would be required to rule out the variable/episodic nature of emission.

5.4 Beamed Emission

The other possible reason for non-detection could be that the Earth was outside the planet’s emission beam. Cyclotron maser emission is known to be confined within a beam. The decameter emission of Jupiter is only detectable over certain rotational phase ranges because the emission is narrowly beamed (O’Gorman et al. 2018; Hallinan et al. 2013).

Assuming that the magnetic axis is aligned with the rotation axis and that emission is produced near the planetary poles, the typical beaming angle is between $50^\circ - 60^\circ$ (Melrose & Dulk 1982; Dulk 1985; Zarka 1998; Treumann 2006). Such beamed emission will only be observable from Earth during a particular phase of the orbit of the exoplanet; our near-complete orbital coverage for HD 41004Bb at 150 MHz partially mitigates this problem. An alternate approach to detect beamed emission is to observe several sources so that in a few cases, the emission is beamed along the line of sight.

5.5 Quenching of emission

If the local plasma frequency, ν_p is too high, the cyclotron emission cannot propagate. For a plasma distribution with density n (in cm^{-3}), the plasma frequency, ν_p is given as

$$\nu_p = \sqrt{\frac{n e^2}{\pi m_e}} \sim 8.98 \text{ kHz} \sqrt{n} \quad (8)$$

The plasma will absorb emission at frequencies lower than the ν_p . For radio emission to be detected, the maximum cyclotron frequency, ν_c within the source region, must be greater than the ν_p at every point along the line of sight such that $\nu_c \gg \nu_p$.

If the above condition is not satisfied, then the radio emission from the exoplanet would be quenched due to the local plasma (Grießmeier et al. 2007b; Hess & Zarka 2011). The number density of electrons n from the stellar wind,

Model	Maximum cyclotron frequency MHz	Modeled flux density mJy	achieved 3σ rms mJy	κ_{\max} –
Stellar Wind Kinetic Energy	125	3	1.8	0.6
Stellar Wind Magnetic Energy	125	64	1.8	0.03
Stellar Wind Kinetic Energy	400	2	0.12	0.06
Stellar Wind Magnetic Energy	400	44	0.12	0.003

Table 2. Summary of the predicted flux density and the 3σ rms sensitivities achieved during our observations. Also shown is the value of κ_{\max} which is the upper limit to the ratio of η_{HD} to that of η_J (see equation 7)

at the position of HD 41004Bb (following (Grießmeier et al. 2004, 2007a; Lynch et al. 2018)) taking the stellar mass, age, spectral type as well as the wind velocity and the orbital distance of the planet into account is $\sim 6.6 \times 10^4 \text{ cm}^{-3}$, that gives $\nu_P = 2.2 \text{ MHz}$, much below the emission frequency.

Further, for close-in hot-Jupiters/ brown dwarfs, the upper layers of the atmosphere are heated by the stellar radiation, leading to an inflated and extended upper atmosphere. The outer layers also become highly ionized, which increases the electron density, resulting in a high plasma frequency. If this frequency exceeds the maximum cyclotron frequency, then the emission will be quenched (also see (Daley-Yates & Stevens 2017, 2018; Weber et al. 2017a,b, 2018)).

6 CONCLUSION

In this paper, we carried out one of the most sensitive radio observations of the HD 41004 field with GMRT at 150 MHz and 400 MHz. We do not detect radio emission from the HD 41004 system. However, we can place a very strong and robust 3σ upper limits of 1.8 mJy at 150 MHz and 0.12 mJy at 400 MHz on the steady-state or quiescence component of the radio emission (provided that the emission is beamed towards us). These are some of the lowest limits achieved at these wavelengths and are much lower than the theoretically predicted flux densities. We have provided some plausible reasons for the non-detection of radio emission from this system.

7 ACKNOWLEDGEMENT

We thank the referee for their insightful comments and suggestions that have resulted in a significant improvement of the manuscript. This work is based on observations made with the Giant Metrewave Radio Telescope, which is operated by the National Centre for Radio Astrophysics of the Tata Institute of Fundamental Research and is located at Khodad, Maharashtra, India. We thank the GMRT staff for efficient support to these observations. We acknowledge the support of the Department of Atomic Energy, Government of India, under the project 12-R&D-TFR-5.02-0700. M.T. is supported by MEXT/JSPS KAKENHI grant Nos. 18H05442, 15H02063, and 22000005. Part of this research

was carried out at the Jet Propulsion Laboratory, California Institute of Technology, under a contract with the National Aeronautics and Space Administration. This research has made use of the NASA Exoplanet Archive, which is operated by the California Institute of Technology, under contract with the National Aeronautics and Space Administration under the Exoplanet Exploration Program. This research has also made use of NASA’s Astrophysics Data System Abstract Service and the SIMBAD database, operated at CDS, Strasbourg, France.

8 DATA AVAILABILITY

The data presented in this article are available on the GMRT archive at <https://naps.ncra.tifr.res.in/goa/>, and can be accessed with proposal ids 17_066 and 35_001.

APPENDIX A: MAGNETIC FIELD OF PLANETS

For solar system planets it has been suggested that the magnetic moment of a planet is proportional to its angular momentum (Farrell et al. 1999).

$$\mu_P \propto L_P \sim \omega_P M_P R_P^2 \quad (\text{A1})$$

where L_P is the angular momentum of the planet, μ_P is the magnetic moment of the planet and R_P , M_P and ω_P are the radius, mass and rotation rate of the planet. For Jupiter,

$$\mu_J \sim \omega_J M_J R_J^2 \quad (\text{A2})$$

and also,

$$\mu_J = 4.2 [G] R_J^3 \quad (\text{A3})$$

from Connerney et al. (1981).

Dividing equation (A1) by equation (A2) and substituting the values from equation (A3)

$$\mu_P = \left(\frac{\omega_P}{\omega_J}\right) \left(\frac{M_P}{M_J}\right) \left(\frac{R_P}{R_J}\right)^2 4.2 [G] R_J^3 \quad (\text{A4})$$

The magnetic field B_P at the poles is given as:

$$B_P = \frac{2\mu_P}{R_P^3} = 8.4 [G] \left(\frac{\omega_P}{\omega_J}\right) \left(\frac{M_P}{M_J}\right) \left(\frac{R_J}{R_P}\right) \quad (\text{A5})$$

and thus, we obtain

$$\nu_c = 2.8 \text{ MHz } [B_P/G] = 23.5 \text{ MHz } \left(\frac{\omega_P}{\omega_J} \right) \left(\frac{M_P}{M_J} \right) \left(\frac{R_J}{R_P} \right) \quad (\text{A6})$$

REFERENCES

- Antonova A., Doyle J. G., Hallinan G., Golden A., Koen C., 2007, *A&A*, **472**, 257
- Bailer-Jones C. A. L., Rybizki J., Fouesneau M., Mantelet G., Andrae R., 2018, *AJ*, **156**, 58
- Bastian T. S., Dulk G. A., Leblanc Y., 2000, *ApJ*, **545**, 1058
- Bastian T. S., Villadsen J., Maps A., Hallinan G., Beasley A. J., 2018, *ApJ*, **857**, 133
- Batalha N. M., et al., 2013, *ApJS*, **204**, 24
- Berger E., et al., 2001, *Nature*, **410**, 338
- Bigg E. K., 1964, *Nature*, **203**, 1008
- Burke B. F., Franklin K. L., 1955, *J. Geophys. Res.*, **60**, 213
- Chen J., Kipping D., 2017, *ApJ*, **834**, 17
- Connerney J. E. P., Acuna M. H., Ness N. F., 1981, *J. Geophys. Res.*, **86**, 8370
- Cumming A., Butler R. P., Marcy G. W., Vogt S. S., Wright J. T., Fischer D. A., 2008, *PASP*, **120**, 531
- Daley-Yates S., Stevens I. R., 2017, *Astronomische Nachrichten*, **338**, 881
- Daley-Yates S., Stevens I. R., 2018, *Contributions of the Astronomical Observatory Skalnaté Pleso*, **48**, 129
- Desch M. D., Kaiser M. L., 1984, *Nature*, **310**, 755
- Dressing C. D., Charbonneau D., 2015, *ApJ*, **807**, 45
- Dulk G. A., 1985, *ARA&A*, **23**, 169
- Farrell W. M., Desch M. D., Zarka P., 1999, *J. Geophys. Res.*, **104**, 14025
- Gaia DR2 Collaboration et al., 2018, *A&A*, **616**, A1
- Gaidos E., Fischer D. A., Mann A. W., Howard A. W., 2013, *ApJ*, **771**, 18
- George S. J., Stevens I. R., 2007, *MNRAS*, **382**, 455
- Gladman B., Quinn D. D., Nicholson P., Rand R., 1996, *Icarus*, **122**, 166
- Gonzalez G., 1997, *MNRAS*, **285**, 403
- Grißmeier J.-M., 2015, in Lammer H., Khodachenko M., eds, *Astrophysics and Space Science Library Vol. 411, Characterizing Stellar and Exoplanetary Environments*. p. 213, doi:10.1007/978-3-319-09749-7_11
- Grißmeier J.-M., 2017, *Planetary Radio Emissions VIII*, pp 285–299
- Grißmeier J. M., 2018, *Future Exoplanet Research: Radio Detection and Characterization, Handbook of Exoplanets*, Edited by Hans J. Deeg and Juan Antonio Belmonte. Springer Living Reference Work, ISBN: 978-3-319-30648-3, 2017, id.9. p. 159, doi:10.1007/978-3-319-55333-7_159
- Grißmeier J.-M., et al., 2004, *A&A*, **425**, 753
- Grißmeier J. M., Preusse S., Khodachenko M., Motschmann U., Mann G., Rucker H. O., 2007a, *Planet. Space Sci.*, **55**, 618
- Grißmeier J.-M., Zarka P., Spreeuw H., 2007b, *A&A*, **475**, 359
- Grißmeier J.-M., Zarka P., Girard J. N., 2011, *Radio Science*, **46**, RS0F09
- Gupta Y., et al., 2017, *Current Science*, **113**, 707
- Hallinan G., et al., 2007, *ApJ*, **663**, L25
- Hallinan G., Antonova A., Doyle J. G., Bourke S., Lane C., Golden A., 2008, *The Astrophysical Journal*, **684**, 644
- Hallinan G., Sirothia S. K., Antonova A., Ishwara-Chandra C. H., Bourke S., Doyle J. G., Hartman J., Golden A., 2013, *ApJ*, **762**, 34
- Hess S. L. G., Zarka P., 2011, *A&A*, **531**, A29
- Intema H. T., 2014a, SPAM: Source Peeling and Atmospheric Modeling, Astrophysics Source Code Library (ascl:1408.006)
- Intema H. T., 2014b, in *Astronomical Society of India Conference Series*. (arXiv:1402.4889)
- Intema H. T., van der Tol S., Cotton W. D., Cohen A. S., van Bommel I. M., Röttgering H. J. A., 2009, *A&A*, **501**, 1185
- Ishwara-Chandra C. H., Taylor A. R., Green D. A., Stil J. M., Vaccari M., Ocran E. F., 2020, arXiv e-prints, p. arXiv:2008.02530
- Jardine M., Collier Cameron A., 2008, *A&A*, **490**, 843
- Kao M. M., Hallinan G., Pineda J. S., Escala I., Burgasser A., Bourke S., Stevenson D., 2016, *ApJ*, **818**, 24
- Lazio T. J. W., 2018, *Radio Observations as an Exoplanet Discovery Method, Handbook of Exoplanets*, Edited by Hans J. Deeg and Juan Antonio Belmonte. Springer Living Reference Work, ISBN: 978-3-319-30648-3, 2017, id.9. p. 9, doi:10.1007/978-3-319-55333-7_9
- Lazio T. J. W., Farrell W. M., 2007, *ApJ*, **668**, 1182
- Lazio T. Joseph W., Farrell W. M., Dietrick J., Greenlees E., Hogan E., Jones C., Hennig L. A., 2004, *ApJ*, **612**, 511
- Lazio T. J. W., Shankland P. D., Farrell W. M., Blank D. L., 2010, *AJ*, **140**, 1929
- Lazio J., et al., 2019, *BAAS*, **51**, 135
- Lecavelier Des Etangs A., Sirothia S. K., Gopal-Krishna Zarka P., 2011, *A&A*, **533**, A50
- Lecavelier des Etangs A., Sirothia S. K., Gopal-Krishna Zarka P., 2013, *A&A*, **552**, A65
- Louis C. K., Hess S. L. G., Cecconi B., Zarka P., Lamy L., Aicardi S., Loh A., 2019, *A&A*, **627**, A30
- Lynch C. R., Murphy T., Lenc E., Kaplan D. L., 2018, *MNRAS*, **478**, 1763
- Marcy G. W., et al., 2014, *ApJS*, **210**, 20
- Melrose D. B., Dulk G. A., 1982, *ApJ*, **259**, 844
- Mulders G. D., 2018, *Planet Populations as a Function of Stellar Properties, Handbook of Exoplanets*, Edited by Hans J. Deeg and Juan Antonio Belmonte. Springer Living Reference Work, ISBN: 978-3-319-30648-3, 2017, id.9. p. 153, doi:10.1007/978-3-319-55333-7_153
- Mulders G. D., Pascucci I., Apai D., 2015, *ApJ*, **814**, 130
- Narang M., Manoj P., Furlan E., Mordasini C., Henning T., Mathew B., Banyal R. K., Sivarani T., 2018, *AJ*, **156**, 221
- Newkirk G. J., 1980, in Pepin R. O., Eddy J. A., Merrill R. B., eds, *The Ancient Sun: Fossil Record in the Earth, Moon and Meteorites*. pp 293–320
- Nichols J. D., Milan S. E., 2016, *MNRAS*, **461**, 2353
- O’Gorman E., Coughlan C. P., Vlemmings W., Varenus E., Sirothia S., Ray T. P., Olofsson H., 2018, *A&A*, **612**, A52
- Parker E. N., 1958, *ApJ*, **128**, 664
- Perryman M., 2011, *The Exoplanet Handbook*
- Pope B. J. S., Bedell M., Callingham J. R., Vedantham H. K., Snellen I. A. G., Price-Whelan A. M., Shimwell T. W., 2020, *ApJ*, **890**, L19
- Reiners A., Christensen U. R., 2010, *A&A*, **522**, A13
- Route M., 2019, *ApJ*, **872**, 79
- Saffe C., Gómez M., Chavero C., 2005, *A&A*, **443**, 609
- Sánchez-Lavega A., 2004, *ApJ*, **609**, L87
- Shkolnik E. L., Llama J., 2018, *Signatures of Star-Planet Interactions, andbook of Exoplanets*, Edited by Hans J. Deeg and Juan Antonio Belmonte. Springer Living Reference Work, ISBN: 978-3-319-30648-3, 2017, id.9. p. 20, doi:10.1007/978-3-319-55333-7_20
- Smith A. M. S., Collier Cameron A., Greaves J., Jardine M., Langston G., Backer D., 2009, *MNRAS*, **395**, 335
- Stroe A., Snellen I. A. G., Röttgering H. J. A., 2012, *A&A*, **546**, A116
- Treumann R. A., 2006, *A&ARv*, **13**, 229
- Vedantham H. K., et al., 2020, *Nature Astronomy*,
- Viswanath G., Narang M., Manoj P., Mathew B., Kartha S. S., 2020, *AJ*, **159**, 194
- Weber C., et al., 2017a, *Planetary Radio Emissions VIII*, pp 317–329

- Weber C., et al., 2017b, *MNRAS*, **469**, 3505
- Weber C., Erkaev N. V., Ivanov V. A., Odert P., Grießmeier J. M., Fossati L., Lammer H., Rucker H. O., 2018, *MNRAS*, **480**, 3680
- Williams P. K. G., Gizis J. E., Berger E., 2017, *ApJ*, **834**, 117
- Winn J. N., 2018, Planet Occurrence: Doppler and Transit Surveys, and book of Exoplanets, Edited by Hans J. Deeg and Juan Antonio Belmonte. Springer Living Reference Work, ISBN: 978-3-319-30648-3, 2017, id.9. p. 195, doi:10.1007/978-3-319-55333-7_195
- Winn J. N., Fabrycky D. C., 2015, *ARA&A*, **53**, 409
- Wolszczan A., Route M., 2014, *ApJ*, **788**, 23
- Wu C. S., Lee L. C., 1979, *ApJ*, **230**, 621
- Yadav R. K., Thorngren D. P., 2017, *ApJ*, **849**, L12
- Zarka P., 1998, *J. Geophys. Res.*, **103**, 20159
- Zarka P., 2000, *Washington DC American Geophysical Union Geophysical Monograph Series*, **119**, 167
- Zarka P., 2007, *Planet. Space Sci.*, **55**, 598
- Zarka P., 2018, Star-Planet Interactions in the Radio Domain: Prospect for Their Detection, Handbook of Exoplanets, Edited by Hans J. Deeg and Juan Antonio Belmonte. Springer Living Reference Work, ISBN: 978-3-319-30648-3, 2017, id.9. p. 22, doi:10.1007/978-3-319-55333-7_22
- Zarka P., et al., 1997, in Rucker H. O., Bauer S. J., Lecacheux A., eds, Planetary Radio Emission IV. pp 101–127
- Zarka P., Treumann R. A., Ryabov B. P., Ryabov V. B., 2001, *Ap&SS*, **277**, 293
- Zarka P., Cecconi B., Kurth W. S., 2004, *Journal of Geophysical Research (Space Physics)*, **109**, A09S15
- Zarka P., Marques M. S., Louis C., Ryabov V. B., Lamy L., Echer E., Cecconi B., 2017, in Fischer G., Mann G., Panchenko M., Zarka P., eds, Planetary Radio Emissions VIII. pp 45–58 ([arXiv:1709.04386](https://arxiv.org/abs/1709.04386)), doi:10.1553/PRE8s45
- Zarka P., Marques M. S., Louis C., Ryabov V. B., Lamy L., Echer E., Cecconi B., 2018, *A&A*, **618**, A84
- Zucker S., Mazeh T., Santos N. C., Udry S., Mayor M., 2004, *A&A*, **426**, 695

This paper has been typeset from a $\text{T}_{\text{E}}\text{X}/\text{L}_{\text{A}}\text{T}_{\text{E}}\text{X}$ file prepared by the author.